Available online at www.sciencedirect.com
SCIENCE DIRECT®
Earth and Planetary Science Letters 240 (2005) 573–588
EPSL
www.elsevier.com/locate/epsl

Refining the noble gas record of the Réunion mantle plume source: Implications on mantle geochemistry

Jens Hopp *, Mario Trieloff

Mineralogisches Institut, Universität Heidelberg, Im Neuenheimer Feld 236, D-69120 Heidelberg, Germany

Received 20 December 2004; received in revised form 9 June 2005; accepted 22 September 2005
Available online 8 November 2005
Editor: V. Courtillot

Abstract

We report isotope analyses of helium, neon, argon, and xenon using different extraction techniques such as stepwise dynamic and static crushing, and high-resolution stepwise heating of three mantle xenoliths from Réunion Island. He and Ne isotopic compositions were similar to previously reported Réunion data, yielding a more radiogenic composition when compared to the Hawaiian or Icelandic mantle plume sources. We furthermore observed correlated $^{129}Xe/^{130}Xe$ and $^{136}Xe/^{130}Xe$ ratios following the mantle trend with maximum values of 6.93 ± 0.14 and 2.36 ± 0.06, respectively. High-resolution argon analyses resulted in maximum $^{40}Ar/^{36}Ar$ ratios of 9000–11,000, in agreement with maximum values obtained in previous studies. We observed a well-defined hyperbolic mixing curve between an atmospheric and a mantle component in a diagram of $^{40}Ar/^{36}Ar$ vs. $^{20}Ne/^{22}Ne$. Using a mantle $^{20}Ne/^{22}Ne$ of 12.5 (Ne–B) a consistent $^{40}Ar/^{36}Ar$ value of $11{,}053 \pm 220$ in sample ILR 84-4 was obtained, whereas extrapolations to a higher mantle $^{20}Ne/^{22}Ne$ ratio of 13.8 (solar wind) would lead to a much higher $^{40}Ar/^{36}Ar$ ratio of 75,000, far above observed maximum values. This favours a mantle $^{20}Ne/^{22}Ne$ of about 12.5 considered to be equivalent to Ne–B. Extrapolated and estimated $^{40}Ar/^{36}Ar$ ratios of the Réunion, Iceland, Loihi, and MORB mantle sources, respectively, tend to be linearly correlated with air corrected $^{21}Ne/^{22}Ne$ and show the same systematic sequence of increasing relative contributions in radiogenic isotopes (Iceland–Loihi–Réunion–MORB) as observed for $^{4}He/^{3}He$. In general, He–Ne–Ar isotope systematics of the oceanic mantle can be explained by following processes: (i) different degree of mixing between pure radiogenic and pure primordial isotopes generating the MORB and primitive plume (Loihi-type) endmembers; (ii) relatively recent fractionation of He relative to Ne and Ar, in one or both endmembers; (iii) after the primary fractionation event, different degrees of mixing between melts or fluids of MORB and primitive plume affinity generate the variety of observed OIB data, also on a local scale; (iv) very late-stage secondary fractionation during magma ascent and magma degassing leads to further strong variation in He/Ne and He/Ar ratios.

Keywords: noble gas isotope systematics; Réunion hotspot; mantle plume sources; binary mixing scenarios

1. Introduction

Noble gas isotopes, especially of Helium, are widely used to distinguish unambiguously between "plume" (mostly assumed to have a deep mantle origin) and shallow mantle sources of volcanic activity. The asthenospheric mantle sampled by mid-ocean ridge basalts (MORB) [1–4] and samples of continental lithospheric origin [5–9] generally show a lower relative contribution of primordial noble gas isotopes (e.g., ^{3}He, $^{20,22}Ne$) compared to hotspot sources like Hawaii (Loihi) [3,10–12] or Iceland [12,13]. However, at

* Corresponding author. Tel.: +49 6221 544895; fax: +49 6221 544805.
E-mail address: jhopp@min.uni-heidelberg.de (J. Hopp).

0012-821X/$ - see front matter © 2005 Elsevier B.V. All rights reserved.
doi:10.1016/j.epsl.2005.09.036

some localities both MORB-type He and plume-type Ne isotopic compositions (i.e., significantly lower excess of nucleogenic ^{21}Ne when compared to MORB) were observed, e.g., at the East Pacific rise [14]. These authors suggested a possible decoupling of He and Ne isotopes, e.g., caused by different time integrated evolution due to distinct initial ^{3}He/^{22}Ne ratios in the respective mantle sources. This interpretation was extended to explain some compositionally intermediate hotspot compositions, e.g., of Réunion Island [15] that displays ^{3}He/^{4}He ≈ 12–13R_A [15–18] ($1R_A$=atmospheric unit) in contrast to MORB values ($8 \pm 1R_A$) or primitive plumes (up to $51R_A$ at Baffin Island [19]). In this view, the rather constant and similar ^{3}He/^{4}He compositions of samples from Réunion and Mauritius (with ^{3}He/^{4}He ≈ 10–11R_A, [15]), the latter representing a former locality of the same hotspot track, were interpreted as indigenous composition of the Réunion mantle plume source exhibiting a characteristic ^{3}He/^{22}Ne ratio [15].

Based on studies of other settings (South Atlantic [20–22]; Iceland [13,23]), a hyperbolic correlation in a ^{4}He/^{3}He vs. ^{21}Ne/^{22}Ne$_{mantle}$ space (Fig. 1, corrected for atmospheric Ne by extrapolation to an assumed mantle endmember value of ^{20}Ne/^{22}Ne, here we use 12.5) was discussed as a result of mixing processes. Thus, we may interpret the individual hyperbolic trends shown in Fig. 1 as mixing curves between a more radiogenic/nucleogenic MORB component with higher ^{4}He/^{3}He and ^{21}Ne/^{22}Ne$_{mantle}$ and a plume component dominated by primordial isotopes. Restricted to a local scale, this can be exemplified at the Hawaiian islands, with Loihi (the youngest volcano of the high ^{3}He/^{4}He hotspot) as primitive endmember [3,10–12] and post-erosional phase volcanics on Oahu with MORB type composition [24]. Kilauea data [10] plot intermediately on the hyperbolic trajectory at ^{4}He/^{3}He ratios of 42,000–58,000. More recent reports on He–Ne compositions of the Galapagos archipelago [25] and the East Pacific Rise [26] do also fit such a local mixing scenario.

The mixing scenario seems a capable model without the need of complex multiple source evolution models that would require different time-integrated evolution paths and different He/Ne compositions yielding a rather well-constrained trend even on a very restricted local scale. Additional evidence for mantle mixing could be provided by extension of isotope systematics to the heavy noble gases Ar and Xe. However, argon and xenon isotope systematics of different mantle sources are only crudely known, mainly because it is rather difficult to discriminate atmospheric contributions [27,28].

To overcome this problem, ^{20}Ne/^{22}Ne ratios can potentially be used as a proxy for atmospheric contam-

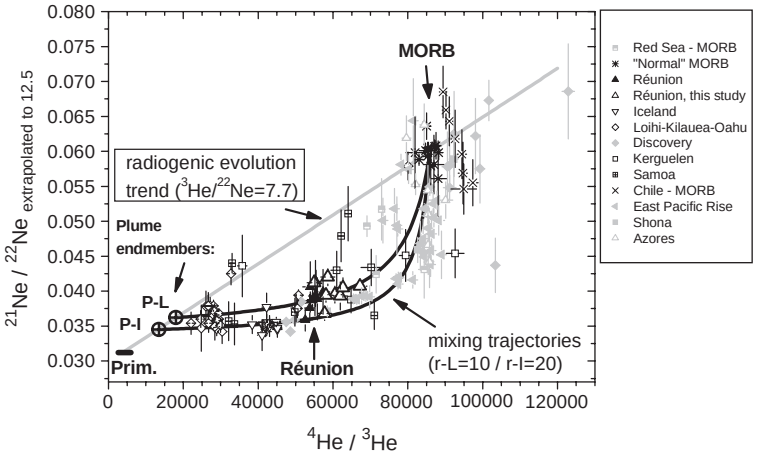

Fig. 1. A ^{21}Ne/^{22}Ne (air corrected with ^{20}Ne/^{22}Ne=12.5) vs. ^{4}He/^{3}He isotope diagram of data from oceanic samples [1,4,10–16,18,20,22,24,39,60–63]. Only data with relative 1σ uncertainties of less than 10% are displayed. In case of data obtained by stepwise heating extraction only total values are used, thus excluding a possible experimentally induced elemental fractionation. Data from MORB not affected by a close to ridge seamount (="plume") are shown with black crosses or stars. Samples from ridge locations typically exhibiting plume–ridge interaction are represented by grey symbols. Off-ridge hotspots and Iceland (example of a primitive plume lying on a ridge) are plotted in black symbols. Réunion data from literature are shown in black filled up-triangles, whereas the results of this study are plotted as black open up-triangles. The radiogenic evolution line is shown in grey (initial ^{3}He/^{22}Ne=7.7; production ratio ^{4}He*/^{21}Ne*=2.2×10^{7}). Hyperbolic trends represent binary mixing between a Loihi-type endmember P-L (^{4}He/^{3}He=18,050 (~40R_A); ^{21}Ne/^{22}Ne$_{corr}$=0.0362) and an Iceland-type endmember P-I (^{4}He/^{3}He=14,000 (~51R_A); ^{21}Ne/^{22}Ne$_{corr}$=0.0345), respectively, with MORB (^{4}He/^{3}He=86,500 (=8.35R_A); ^{21}Ne/^{22}Ne$_{corr}$=0.06), with a fractionation factor r-L=10 and r-I=20 (r=(^{3}He/^{22}Ne$_{MORB}$)/(^{3}He/^{22}Ne$_{plume}$)) [64]. Initial slightly differently evolved plume endmember compositions are shown as open circles.

ination. The atmospheric $^{20}Ne/^{22}Ne$ ratio of 9.8 differs significantly from the mantle $^{20}Ne/^{22}Ne$ ratio, which is here assumed to be equivalent to a meteoritic component called Ne–B ($=12.52\pm0.18$ [29]). This component represents a surface implanted mixture of low and high energetic solar wind particles commonly observed in meteorites. Alternative scenarios propose a value of about 13.80 ± 0.05 [30] corresponding to the unfractionated (low energetic) solar wind composition thought to represent the solar nebula gas. A simple binary mixing between atmospheric and mantle fluids then should lead to correlated isotope ratios of $^{40}Ar/^{36}Ar$ and $^{129,\ 131-136}Xe/^{130}Xe$, respectively, plotted against measured $^{20}Ne/^{22}Ne$ ratios. This correlation should be hyperbolic, with the curvature depending on the ratio of the elemental ratios of both endmembers (atmospheric and mantle). Extrapolation to the chosen $^{20}Ne/^{22}Ne$-mantle ratio then yields the corresponding mantle ratios in $^{40}Ar/^{36}Ar$ and other isotope ratios. This is valid only in case of a simple two-component mixture between an atmospheric and a mantle component. Another precondition of a successful deconvolution of a mantle and an atmospheric component is several high-quality $^{20}Ne/^{22}Ne$ data points obtained on individual samples. Buikin et al. [9] have shown that every single sample even from one outcrop displays an individual hyperbolic correlation.

Another approach to assess mantle $^{40}Ar/^{36}Ar$ ratios uses high-resolution stepwise heating and crushing extractions to determine the maximum excess relative to atmospheric composition. Unfortunately, due to generally low concentrations of xenon in mantle rocks, this procedure is still restricted to argon and can only provide a lower limit for the respective $^{40}Ar/^{36}Ar$ mantle composition and needs a lot of data from the respective mantle reservoirs before compelling conclusions can be reached.

In this study, we reanalysed three xenolith samples from the Réunion hotspot with both procedures mentioned above. Réunion is of special interest in noble gas geochemistry, because it is characterized by a very homogeneous helium and neon isotopic composition that is intermediate relative to the other main mantle components, MORB and the primordial endmember currently best defined by Loihi samples (see Fig. 1). Hence, the Réunion hotspot can serve as an ideal compositional tie for the heavy noble gas isotopes.

All three analysed samples previously displayed a clear mantle signature and showed $^{4}He/^{40}Ar^{*}$ ratios in the range of expected mantle production ratios [16] and are thus assumed to represent a largely unfractionated mantle source composition. Additional information about the carrier phases of mantle and atmospheric argon in the samples were obtained by high-resolution stepwise static crushing and stepwise heating analyses on neutron-irradiated samples as commonly used for ^{40}Ar–^{39}Ar-dating. Thus, we could monitor the degassing of Ca-, Cl-, and K-bearing phases by analysing irradiation-derived ^{37}Ar, ^{38}Ar, and ^{39}Ar, respectively. In addition, noble gas isotopic compositions of the non-irradiated samples were obtained by stepwise dynamic crushing in ball mills.

2. Samples and experimental methods

The current location of the Réunion hotspot in the Indian Ocean, the volcano Piton de la Fournaise, is one of the most active volcanoes in the world. All samples stem from Piton Chisny in the Plaine de Sables from a ~2.3-ka-old eruption, located 4.5 km west of the currently active Piton de la Fournaise and had been investigated in a previous study [16]. Xenolith ILR 84-4 is described as a harzburgite, ILR 84-6 and Chisny 88-1 are dunites [16]. All samples contain small amounts of calcic pyroxene. Single grains of orthopyroxene are only found in thin section of sample Chisny 88-1, but not in ILR 84-4 that is classified as harzburgite, but this does not prove its absence. The olivines are characterized by a uniform Mg# of 0.84–0.85. Because of their restitic character all samples are regarded as cumulate rocks [31]. The fluid inclusions in ILR 84-4 were trapped in 6–9 km depth, as revealed by microthermometry [31], i.e., entrapment of the fluids occurred at the interface between oceanic crust and upper mantle.

All analysed samples were grain separates of hand-picked olivine grains (>500 μm) that appeared free of alteration, but still could contain some inclusions (e.g., pyroxenes, melt inclusions). For argon analyses (of neutron-irradiated samples), ILR 84-4 olivine was divided in two samples showing lower and higher abundances in fluid inclusions. This should help resolving the fluid inclusion signature. Before measurements/irradiation, all samples had been cleaned using diluted nitric acid, deionized water and ethanol.

2.1. Ar analyses (irradiated samples)

All samples had been neutron-irradiated without Cd shielding in the GKSS-Reaktor at Geesthacht, Germany. To avoid significant production of ^{36}Ar from ^{40}Ca, the irradiation time was restricted to 2 days. We used seven NL25 hornblende standards as irradiation

monitors (standard age 2.66 Ga) [32] and, for determination of Ca and Cl concentrations and correction factors, two CaF_2 standards and one Cl standard (Pyrex glass). The resulting J value was 0.00065 ± 0.00002.

Argon in the irradiated samples was extracted by both high-resolution stepwise heating in an inductively heated furnace and by stepwise crushing in a static crusher [33]. The gas was purified using a hot (=700 °C) and a cold Ti getter, and several hot (=400 °C) and cold Zr–Al–(SAES) getters. Subsequent isotope analyses were performed with a CH5 mass spectrometer. Correction for instrumental mass fractionation was assured by repeated analyses of standard gas with isotopic composition of air. Blank level of ^{40}Ar depended on extraction temperature and varied between ca. 10^{-10} (cold) and 9×10^{-8} (maximum value at 1750 °C) cm^3 STP/g. The blank showed an air-like isotopic composition.

2.2. He–Ne–Ar–Xe analyses (non-irradiated samples)

To separate a mantle fluid component from in situ radiogenic or possible cosmogenic contributions sited in the mineral lattice (e.g., [34]), noble gases were released by sequential dynamic crushing in three simultaneously driven ball mills. After gas extraction and purification, argon and xenon were separated at a charcoal cooled with liquid nitrogen. Subsequently, helium and neon were fixed at a cryogenically cooled second charcoal at ca. 11 K. For the cryogenic separation of helium and neon, we used a temperature of 30 K and subsequently extracted neon at 60 K to avoid any release of possible residual argon. Argon and xenon were separated cryogenically at −50 °C using a mixture of ethanol and liquid nitrogen. During xenon measurements, we monitored ^{38}Ar for the determination of separation quality. Generally, the Xe yield was ~100%, whereas about 7% Ar was lost into the Xe fraction. Furthermore, to avoid a high background of ^{40}Ar signal during neon analyses, not all the argon was introduced into the mass spectrometer. Absolute amounts therefore are corrected with the respective dilution factors obtained by calibration measurements. Noble gas isotopic compositions were determined in an in-house modified VG3600 mass spectrometer by measurement with a Faraday cup (^4He, ^{40}Ar, ^{36}Ar) and by single ion counting (for all other isotopes, including ^{36}Ar) at the Max-Planck-Institut für Kernphysik (Heidelberg). In the case of neon measurements, interference corrections ($^{40}Ar^{++}$, mass 42^{++}, CO_2^+) were applied. Before gas inlet, spectrometer background was monitored. For interfering species of mass 42^{++} and CO_2^{++}, we never observed significant change after gas inlet. $^{40}Ar^{++}$ interference corrections in typical sample extractions were less than 1% of the ^{20}Ne background signal. Simultaneous measurements of background ^4He and ^{40}Ar with single ion counting and Faraday cup revealed the ratio between counting and Faraday signal, and in case of argon, served as an independent control in addition to the simultaneous measurement of ^{36}Ar with both, single ion counting and Faraday cup. We used repeated measurements of standard gases with the isotopic composition of air (Ne, Ar, Xe) and a $^3He/^4He = 14.7R_A$ (Potsdam standard), respectively, for correction of experimentally induced mass fractionation effects and for calculation of absolute concentrations. System blank heights were $6–8 \times 10^{-9}$ cm^3 STP (^4He), ca. 3×10^{-12} cm^3 STP (^{20}Ne), $2–3 \times 10^{-12}$ cm^3 STP (^{36}Ar), and $0.8–2.3 \times 10^{-14}$ cm^3 STP (^{132}Xe), respectively. For blank correction, we used the isotopic composition of air [35].

3. Results

3.1. Helium

$^3He/^4He$ ratios are uniformly in the range of 11.5–13.1, except for the last crushing steps of samples ILR 84-4 and ILR 84-6, which show lower $^3He/^4He$ ratios (Fig. 2; Table 1). This might reflect the presence of radiogenic $^4He^*$ in lattice sites that are released in the course of a high number of strokes. However, this would require accumulation of a rather large amount of radiogenic $^4He^*$ in ca. 2300 yr (7×10^{-8} and 10^{-8} cm^3 STP/g for ILR 84-4 and ILR 84-6, respectively,

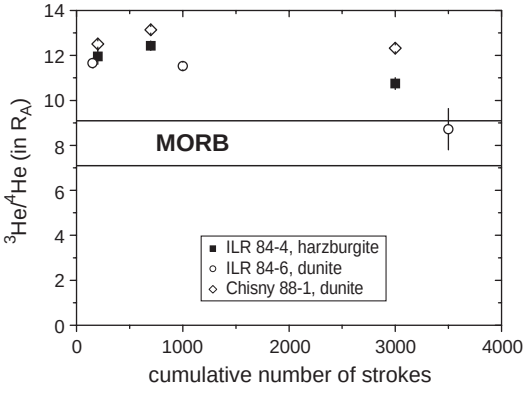

Fig. 2. Obtained $^3He/^4He$ ratios plotted against the cumulative number of strokes (dynamic crushing). Uncertainties are 1σ. Except for last crushing extractions of ILR 84-4 and of ILR 84-6 $^3He/^4He$-ratios are between 11.5 and $13.1R_A$ and thus in the typical range previously obtained for Réunion samples.

Table 1
Results of stepwise dynamic crushing for He, Ne, and Ar analyses of mantle xenoliths from Réunion island

Extraction[a]	^{4}He (10^{-7})[b]	^{4}He/^{3}He	^{3}He/^{4}He (in R_A)[c]	^{22}Ne (10^{-12})[b]	^{20}Ne/^{22}Ne	^{21}Ne/^{22}Ne	^{36}Ar (10^{-11})[b]	^{40}Ar/^{36}Ar	^{4}He/^{40}Ar*
ILR 84-4 harzburgite, 6.911 g									
200×	4.50 (5)	60462 (1726)	11.95 (34)	13.90 (4)	10.52 (3)	0.0318 (3)	22.30 (50)	1633 (33)	1.47 (9)
700×	4.01 (5)	58146 (994)	12.43 (21)	6.30 (3)	11.33 (5)	0.0349 (4)	8.07 (18)	3714 (74)	1.67 (9)
3000×	3.75 (4)	67208 (1645)	10.75 (26)	4.53 (2)	11.70 (5)	0.0372 (5)	4.62 (10)	5536 (111)	1.53 (14)
ILR 84-6 dunite, 5.0384 g									
150×	1.05 (8)	61988 (1094)	11.66 (21)	2.61 (2)	10.77 (10)	0.0325 (6)	4.63 (12)	1949 (35)	1.35 (12)
1000×	1.48 (12)	62661 (933)	11.53 (17)	2.29 (2)	11.61 (10)	0.0368 (8)	2.86 (8)	4548 (82)	1.19 (10)
3500×	0.43 (3)	82880 (8700)	8.72 (92)	0.64 (2)	11.65 (29)	0.0368 (21)	0.77 (2)	4789 (87)	1.09 (13)
Chisny 88-1 dunite, 7.0461 g									
200×	4.03 (3)	57745 (642)	12.51 (14)	8.68 (3)	10.77 (4)	0.0318 (3)	14.05 (43)	1577 (29)	2.18 (14)
700×	3.30 (2)	54984 (627)	13.14 (15)	4.12 (2)	11.11 (5)	0.0349 (4)	5.09 (18)	3326 (62)	2.14 (14)
3000×	2.60 (2)	58642 (690)	12.32 (15)	2.45 (2)	11.29 (7)	0.0362 (6)	2.98 (8)	3923 (71)	2.33 (8)
AIR		722543	≡1		9.8	0.0290		296	

All uncertainties are 1σ uncertainties and include blank correction, correction for experimentally induced mass fractionation, volume corrections (only Ar) and interference corrections in case of neon. An atmospheric value of ^{3}He/^{4}He = 1.384×10^{-6} [65] was used for normalization. Given uncertainties of absolute concentrations and ^{4}He/^{40}Ar* ratios are only statistical errors, whereas uncertainty in absolute concentration of the respective calibration gases are assumed to be 20%. ^{4}He/^{40}Ar* ratios are calculated assuming all ^{36}Ar is atmospheric in origin.

[a] Cumulative number of strokes.

[b] In cm^3 STP/g.

[c] $1R_A = 1.384 \times 10^{-6}$ [65].

compared to initial ^{3}He/^{4}He = $12.5R_A$), corresponding to 20–120 ppm U (with Th/U = 4). This is highly unlikely, because even an amount of 1% accessory alterations (which seems a very high value in view of the fresh samples and the procedure of handpicking), this requires very high U concentrations of 0.2–1.2% in such a contaminating phase. Alternatively, we might have underestimated the ^{4}He blank that could be progressively increased in the course of crushing. However, ^{4}He*/^{40}Ar* ratios of all samples (Table 1) show no significant intrasample variations. ^{3}He/^{4}He and ^{4}He/^{40}Ar* ratios of a previous study [16] are also in broad agreement with results from this study—the values obtained by Staudacher et al. [16] scatter even more. Thus, we suggest that slight intrasample variations could be real among our samples. The highest ^{3}He/^{4}He ratios observed in the first extractions are somewhat lower than previous results [16]; however, within the relatively high uncertainties, we cannot infer a significant discrepancy.

3.2. Neon

In a neon three-isotope diagram (Fig. 3), our results (Table 1) plot within the array that has been observed in previous studies [15,16,18] and that is interpreted as mixing between an atmospheric component and a mantle component with a higher value of ^{20}Ne/^{22}Ne. The position of this array again demonstrates that the Réunion mantle plume source is characterized by an intermediate ^{21}Ne/^{22}Ne composition with respect to more primitive plume sources (e.g., Loihi) and the MORB source (the respective mixing trends are shown in Fig. 3 for comparison). Note that for most extractions, we obtained fairly precise ^{20}Ne/^{22}Ne ratios, which is important for constraining the isotopic composition of the heavier rare gases.

In Fig. 1, air-corrected values of ^{21}Ne/^{22}Ne$_{mantle}$ (using a mantle endmember value of ^{20}Ne/^{22}Ne = 12.5) are plotted against ^{4}He/^{3}He ratios. No significant isoto-

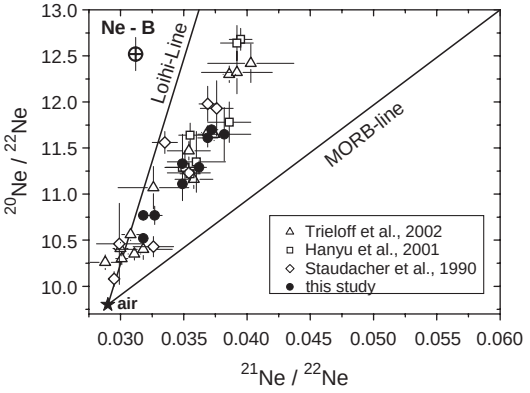

Fig. 3. Neon three isotope plot with data of this study (black filled circles) and data from literature (open symbols) [15,16,18] visualizing a good agreement. Ne–B value is taken from [45]. Errors again are 1σ uncertainties.

pic variations in air-corrected $^{21}Ne/^{22}Ne$ ratios of Réunion samples could be detected (see Fig. 1). Comparison of our results with literature data of several oceanic mantle sources including Réunion well agree with the general observed hyperbolic trends.

3.3. Argon: High-resolution stepwise heating and crushing experiments (irradiated samples)

3.3.1. Degassing pattern

Generally, all samples show a very similar degassing pattern (Table 2), which is not surprising regarding their similar modal composition. In Fig. 4A and B, we show the fractional release (normalized to temperature step ΔT) plotted against extraction temperature for ^{40}Ar and Ca-derived ^{37}Ar. All samples display their main ^{40}Ar release at 1600 °C, related to the melting of olivine. Pyroxene degassing occurs between 1250 °C and 1450 °C and is accompanied by a high amount of ^{37}Ar, indicative of this Ca-bearing phase. Interestingly, ^{37}Ar (and ^{38}Ar, ^{39}Ar) also shows a sharp release peak during olivine melting. Since we know that pyroxene degasses at lower temperatures, these release peaks point to the presence of pyroxene or, alternatively, melt inclusions enclosed in olivine. At low temperatures, only ILR 84-4 displayed a significant release peak of ^{40}Ar (and ^{36}Ar). At intermediate temperatures (ca. 800–1250 °C), the data indicate some amounts of chlorine and potassium, possibly due to interaction with melt from the host magma trapped in veins or some hydrous phases (e.g., serpentine, amphibole) that already had been identified in a previous study on mantle peridotites/pyroxenites [36].

3.3.2. Radiogenic contributions of ^{40}Ar

K concentrations are generally low (less than 20 ppm) and the ^{40}Ar concentrations corrected for air (assuming all ^{36}Ar is of atmospheric origin) are relatively high ($0.5–1\times10^{-6}$ cm^3 STP/g). Calculated apparent ages partly exceed the age of the Earth (Table 2) (for the main release extractions, >1200 °C) and are clearly due to excess (mantle) ^{40}Ar. An in situ radiogenic contribution is therefore negligible.

3.3.3. $^{40}Ar/^{36}Ar$ ratios

Observed $^{40}Ar/^{36}Ar$ ratios in the stepwise heating experiments varied between low atmosphere-like ratios and high values indicative of a mantle component (Fig. 5A, Table 2). The highest values are observed at high temperatures (pyroxene and olivine release peaks, $^{40}Ar/^{36}Ar$ ratios ca. 9000–11,000) and–in case of ILR 84-4–at low temperatures (500–800 °C). For this sample, we observed a significant difference in $^{40}Ar/^{36}Ar$ ratios at low temperatures between the inclusion-rich ($^{40}Ar/^{36}Ar$ ratios ca. 5000–8000) and inclusion-poor aliquot ($^{40}Ar/^{36}Ar$ ratios ca. 3000–5800). We therefore attribute this release peak to decrepitating fluid inclusions that are dominated by a mantle argon component. Residual fluid inclusions or, alternatively, melt inclusions, could then be responsible for the main release at high temperatures. The observed drop in $^{40}Ar/^{36}Ar$ ratios below 2000 at intermediate temperatures seems to be associated with phases formed by the interaction with the host magma, especially because Ar sited in alterations/melt veins is expected to be released at somewhat lower temperatures.

We also analysed Ar released by using a static crushing device for two irradiated samples (ILR 84-4 and Chisny 88-1). With increasing pressure, we observed increasing $^{40}Ar/^{36}Ar$ ratios, yielding maximum values of 9000–10,000 for both samples (Fig. 5B).

3.4. Argon: stepwise crushing experiments (non-irradiated samples)

In a second approach, we use $^{20}Ne/^{22}Ne$ ratios as proxy for contributions of atmospheric argon (Table 1). As can be seen in a diagram $^{40}Ar/^{36}Ar$ vs. $^{20}Ne/^{22}Ne$ (Fig. 6), the results for sample ILR 84-4 are positively correlated and follow a hyperbolic trend. Results for the other two samples follow the same curve, though not as well defined as ILR 84-4 data. In case of simple binary mixing between an atmospheric and a mantle component, we expect such a correlation between $^{40}Ar/^{36}Ar$ and $^{20}Ne/^{22}Ne$ that should follow a hyperbola with a curvature determined by the ratio r of the $^{36}Ar/^{22}Ne$ ratios of the respective endmembers. If both endmember components have equal $^{36}Ar/^{22}Ne$ ratios ($r=1$), this correlation should be linear. Extrapolation of the mixing hyperbola to a mantle $^{20}Ne/^{22}Ne$ ratio (here assumed to be 12.5) then will yield the corresponding mantle endmember $^{40}Ar/^{36}Ar$. Therefore, we performed a least square regression analysis and calculated the best hyperbola function for the samples ILR 84-4, Chisny 88-1, and all samples together, respectively. We obtained for ILR 84-4 a mantle endmember $^{40}Ar/^{36}Ar = 11{,}053 \pm 220$ and $r = 0.380 \pm 0.011$ with $\chi^2 = 2.664$ and a correlation coefficient $R^2 = 0.992$. Regression analysis diverged for Chisny 88-1. Fitting all data, we obtained a mantle endmember $^{40}Ar/^{36}Ar = 14{,}277 \pm 280$ and $r = 0.238 \pm 0.007$, with a rather high $\chi^2 = 41.96$ and a low correlation coefficient $R^2 = 0.837$, favouring the first solution as the best ap-

Table 2
^{40}Ar and $^{40}Ar/^{36}Ar$ results of stepwise heating and stepwise static crushing on irradiated samples

Temperature (°C)	^{40}Ar (10^{-10})[a]	$^{40}Ar/^{36}Ar$	Apparent age (Ma)	Temperature (°C)	^{40}Ar (10^{-10})[a]	$^{40}Ar/^{36}Ar$	Apparent age (Ma)
ILR 84-4 harzburgite, inclusion rich, 428.1 mg (K = 12 ± 2 ppm; Ca = 600 ± 90 ppm; Cl ~ 0.2 ppm)				ILR 84-4 harzburgite, inclusion poor, 842.4 mg (K = 17 ± 1 ppm; Ca = 1450 ± 140 ppm; Cl ~ 0.6 ppm)			
500	101 (3)	8470 (3850)	–	500	44 (2)	4800 (1360)	2688 (842)
580	457 (19)	5790 (470)	5274 (1334)	590	398 (13)	3650 (130)	5538 (813)
660	782 (33)	8430 (540)	7372 (3645)	680	489 (16)	3790 (150)	2708 (112)
730	528 (22)	7340 (620)	3416 (317)	770	114 (4)	3010 (250)	931 (40)
800	185 (8)	8190 (1720)	2038 (215)	860	86 (4)	5760 (1350)	754 (27)
890	182 (8)	10,500 (5230)	2253 (334)	950	33 (1)	2030 (380)	415 (34)
980	173 (7)	1480 (70)	2696 (676)	1040	43 (2)	1190 (110)	594 (54)
1070	113 (2)	2620 (340)	1320 (185)	1130	141 (6)	1510 (70)	1012 (48)
1150	182 (3)	3960 (540)	4127 (1523)	1210	232 (10)	2050 (70)	1878 (140)
1230	575 (9)	2590 (100)	–	1280	279 (12)	4840 (350)	3381 (270)
1290	458 (7)	2930 (140)	4361 (648)	1350	371 (16)	4910 (270)	5070 (799)
1350	546 (9)	7240 (800)	–	1420	484 (20)	8180 (650)	4189 (244)
1410	584 (10)	10,800 (2050)	4761 (797)	1490	555 (23)	5000 (280)	4377 (372)
1470	715 (12)	9160 (1400)	4392 (432)	1550	598 (13)	9980 (1620)	9651 (5598)
1530	1081 (18)	6510 (670)	3751 (251)	1610	1252 (28)	6800 (550)	7368 (874)
1580	1657 (28)	8300 (1040)	5410 (500)	1680	1348 (31)	6070 (820)	5206 (372)
1630	1489 (27)	5930 (910)	4897 (448)	1750	19 (16)	–	–
1690	113 (20)	–	–				

Temperature (°C)	^{40}Ar (10^{-10})[a]	$^{40}Ar/^{36}Ar$	Apparent age (Ma)	Temperature (°C)	^{40}Ar (10^{-10})[a]	$^{40}Ar/^{36}Ar$	Apparent age (Ma)
ILR 84-6 dunite; 1092.9 mg (K ~ 6 ppm; Ca = 660 ± 70 ppm; Cl ~ 0.2 ppm)				Chisny 88-1, dunite; 1196.6 mg (K ~ 9 ppm; Ca = 500 ± 50 ppm; Cl ~ 0.7 ppm)			
320	18 (3)	–	616 (437)	520	43 (2)	421 (67)	212 (113)
420	106 (4)	–	895 (202)	610	124 (3)	324 (13)	–
520	483 (10)	1820 (130)	1592 (124)	700	90 (3)	403 (31)	112 (26)
610	196 (5)	6610 (3970)	2325 (776)	790	686 (15)	799 (21)	1210 (64)
700	33 (3)	911 (434)	154 (40)	880	1981 (43)	3010 (100)	2299 (81)
790	126 (4)	1210 (190)	523 (60)	970	449 (10)	1320 (80)	863 (45)
880	79 (4)	800 (233)	185 (37)	1060	477 (11)	1050 (50)	801 (53)
970	170 (5)	2190 (660)	908 (111)	1150	707 (16)	4840 (700)	1688 (150)
1060	92 (4)	3020 (2020)	232 (23)	1230	1593 (35)	4620 (240)	2438 (172)
1150	559 (12)	683 (21)	1430 (179)	1300	2661 (58)	8710 (600)	5619 (726)
1230	621 (13)	4080 (690)	1800 (194)	1370	2578 (20)	8150 (750)	4395 (370)
1300	959 (20)	6230 (1040)	5272 (1896)	1440	2574 (20)	9470 (1020)	4446 (472)
1370	1298 (27)	2340 (130)	4927 (542)	1510	2586 (22)	11,700 (2140)	5166 (532)
1440	1177 (26)	11,700 (4810)	3509 (357)	1570	7187 (55)	8830 (680)	4690 (173)
1510	1116 (28)	–	3384 (387)	1630	13,730 (110)	5390 (220)	4142 (94)
1570	3261 (67)	8400 (1820)	6180 (1101)	1690	357 (48)	702 (216)	–
1630	5520 (110)	5650 (810)	5305 (556)	1750	128 (82)	–	–
1690	250 (92)	–	1959 (1361)				

Crushing step	^{40}Ar [10^{-11}][a]	$^{40}Ar/^{36}Ar$	Crushing step	^{40}Ar [10^{-11}][a]	$^{40}Ar/^{36}Ar$
ILR 84-4, harzburgite, 283.9 mg			Chisny 88-1, dunite, 507.2 mg		
1	304 (13)	6090 (4750)	1	182 (10)	1570 (26)
2	1944 (64)	6360 (895)	2	447 (22)	2870 (40)
3	13,600 (440)	5180 (107)	3	599 (29)	5320 (100)
4	10,950 (350)	6850 (205)	4	353 (18)	5000 (140)
5	12,180 (390)	7020 (208)	5	221 (28)	9430 (730)
6	2768 (7)	9600 (1310)	6	412 (4)	8820 (380)

Uncertainties include blank correction, correction for experimentally induced mass fractionation, decay and interference correction. Results of other isotopes [36–39] Ar can be obtained from the first author upon request.

[a] In cm^3 STP/g.

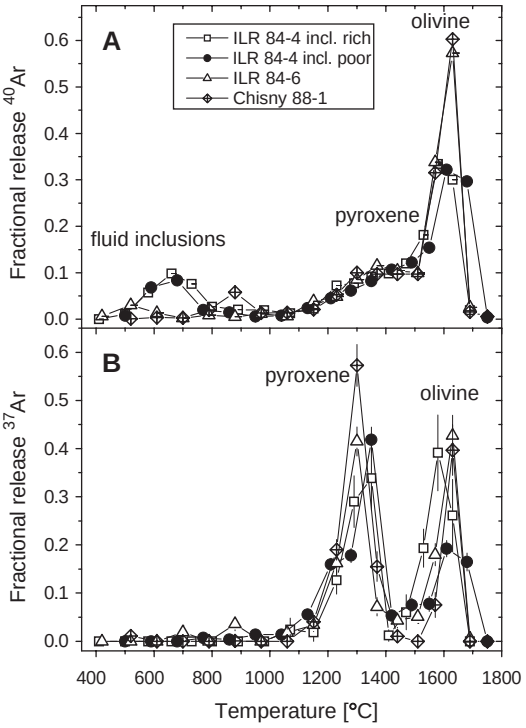

Fig. 4. (A) High-resolution stepwise heating degassing pattern of ^{40}Ar (normalized to temperature step ΔT) (irradiated samples). Uncertainties are 1σ. Main characteristic is the large peak at 1600 °C (olivine), and the less significant peak at 1250–1450 °C (pyroxenes) and, in case of sample ILR 84-4 (inclusion-rich and inclusion-poor sample), a small peak at low temperature assigned to decripitating fluid inclusions. (B) Same as (A) but for Ca-derived ^{37}Ar. Now the pyroxene degassing is clearly visible (mainly clinopyroxene, at slightly lower temperatures than orthopyroxene). ^{37}Ar release at olivine breakdown demonstrates the occurrence of pyroxene ingrowths or melt inclusions in olivine that could not degas at lower temperatures.

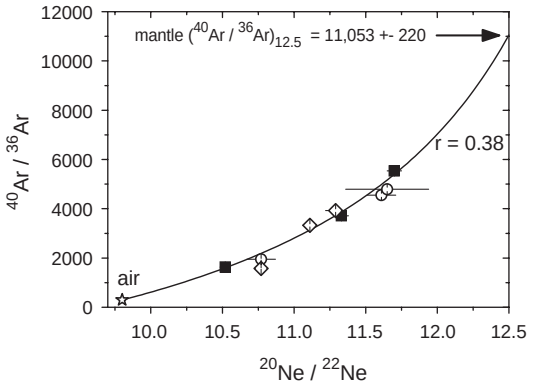

Fig. 6. Measured ^{40}Ar/^{36}Ar ratios plotted vs. ^{20}Ne/^{22}Ne (1σ error). We observe a good correlation for sample ILR 84-4, but less convincing for the other two samples. Nevertheless, all data agree well with calculated hyperbolic trend shown (least square fit; only data of sample ILR 84-4). Result of fit yielded a mantle ^{40}Ar/^{36}Ar = 11,053 ± 220 (at ^{20}Ne/^{22}Ne = 12.5). Corresponding r-value is 0.380 ± 0.003. Symbols as in Fig. 2.

proximation to the Réunion mantle source composition. Of course, we have to be aware that this estimate of the Réunion source composition bases on one sample. Therefore, one might argue that using the data of all three analysed samples yields a more confident value, even if its uncertainty is much higher. However, the possible presence of different atmospheric or mantle ^{36}Ar/^{22}Ne ratios present in the different samples (as shown by Buikin et al. [9]) could introduce further systematic errors. Thus, we need more sample-specific hyperbolic extrapolations [9] for a larger suite of samples in a comparable way as it is done in this study to test the reliability of our result.

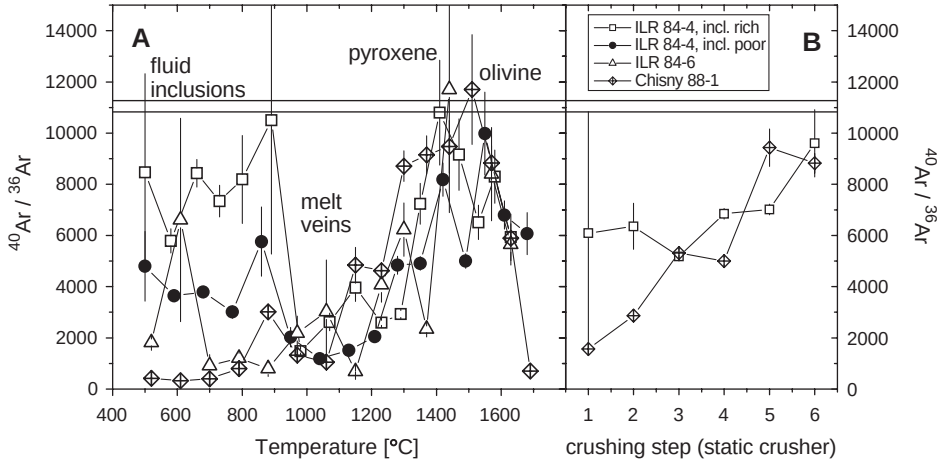

Fig. 5. (A) ^{40}Ar/^{36}Ar ratios vs. temperature with maxima at high temperatures (olivine, pyroxene degassing) and (ILR 84-4) low temperatures (decripitating fluid inclusions). Maximum obtained values of 9000–11,000 are inside their shown 1σ uncertainties in agreement with calculated mantle ^{40}Ar/^{36}Ar ratio of 11,053 ± 220 (see Fig. 6) that is indicated by its upper and lower 1σ line. (B) ^{40}Ar/^{36}Ar-results of static crushing vs. crushing step (samples ILR 84-4 and Chisny 88-1). The ^{40}Ar/^{36}Ar-ratios increase with increasing crushing step up to values of 9000–10,000. Inside their 1σ uncertainties, there is good agreement with results of heating and the calculated mantle ^{40}Ar/^{36}Ar.

An additional test of the calculated fit curves is principally possible if we look at the measured $^{36}Ar/^{22}Ne$ ratios plotted against $^{20}Ne/^{22}Ne$ (Fig. 7). The expected mixing trend between the atmospheric and mantle component should connect $^{36}Ar/^{22}Ne$ values in accordance to the calculated value of r, i.e., the ratio of the respective endmember $^{36}Ar/^{22}Ne$ ratios (mantle/atmospheric value) should be 0.380 or 0.238, respectively. With $r=0.38$ (first solution), a rather well-defined mixing line between a slightly fractionated atmospheric composition of 20 and a mantle $^{36}Ar/^{22}Ne$ of about 7.6 can be drawn (dashed line in Fig. 7). We found no evidence for the presence of additional atmospheric components with a distinct elemental composition. Note that the atmospheric $^{36}Ar/^{22}Ne$ ratio appears only slightly fractionated and rather constant in all our samples. A possible mixing trend between unfractionated air (18.7 [35]) and mantle (9.2 ± 3.0 [18]) is shown for comparison (solid line).

3.5. Xenon isotopes

We observe a linearily correlated excess of ^{129}Xe and ^{136}Xe relative to the unradiogenic ^{130}Xe (Fig. 8; Table 3) that is typical for oceanic mantle samples of different provenance (MORB [2,37,38], Loihi, Iceland [12], Samoa [39]) and previously also had been reported for Réunion samples [18]. The maximum

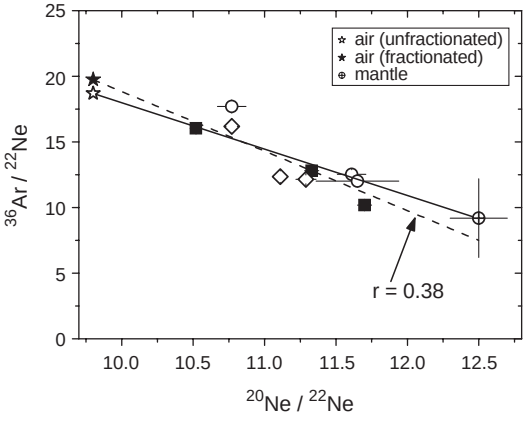

Fig. 7. Diagram showing the elemental $^{36}Ar/^{22}Ne$ ratios vs. $^{20}Ne/^{22}Ne$ (1σ error, symbols as Fig. 2). A proposed mantle $^{36}Ar/^{22}Ne$ value of 9.2 ± 3.0 is shown as a crossed circle. Unfractionated air and a slightly fractionated atmospheric endmember are plotted as open and filled stars, respectively. An expected mixing line between unfractionated air and mantle is shown as a solid line (representing an r-value of about 0.49), but apparently is not in very good agreement. To account better for the data and the calculated r-value of 0.38 (=ratio of $^{36}Ar/^{22}Ne$ ratios of mantle and atmospheric components) a modified mixing line (dashed line) towards a slightly different atmospheric and mantle endmember is drawn.

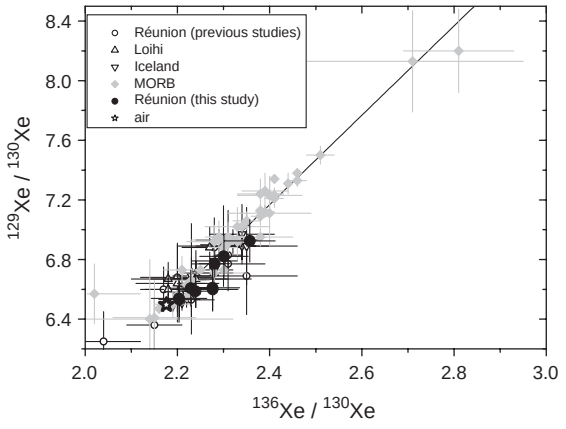

Fig. 8. Xenon three isotope plot with results of this study (filled black circles) and results from previous studies on Réunion samples and other oceanic locations (MORB [2,38]; Iceland, Loihi [12]) (1σ uncertainties). Apparently, our data follow the same mantle trend as previously reported, but show similar to other OIBs a lower excess in ^{129}Xe and ^{136}Xe compared to MORB.

$^{129}Xe/^{130}Xe$ and $^{136}Xe/^{130}Xe$ ratios (6.93 ± 0.14 and 2.36 ± 0.06, sample ILR 84-4) are much lower than observed maximum ratios in MORB and similar to the maximum values found in samples of Iceland and Loihi, but with lower associated $^{20}Ne/^{22}Ne$ ratios in the case of the Réunion sample. We found no simple correlation between $^{129}Xe/^{130}Xe$ and $^{20}Ne/^{22}Ne$. Furthermore, with increasing number of strokes the Xe isotopic composition reflected higher contributions of atmosphere type xenon, though $^{20}Ne/^{22}Ne$ was still rising. This makes an increasing contribution of a fractionated atmospheric component with an elevated Xe/Ne ratio highly probable and most likely resulted from an increasing blank contribution from the tubes in the course of the increasing friction during later stages of stepwise crushing. Alternatively, some minor alteration phases that could be present might preferentially release a fractionated atmospheric component sited in the lattice or in small inclusions at a high number of strokes.

We also measured the isotopes ^{131}Xe, ^{132}Xe, and ^{134}Xe. They share the same general characteristics as described for ^{129}Xe and ^{136}Xe and therefore are not discussed further.

4. Discussion

4.1. Comparison of mantle $^{40}Ar/^{36}Ar$ ratios and inferences for the $^{20}Ne/^{22}Ne$ ratio in the Earth's interior

Our high-resolution stepwise heating results revealed consistent maximum $^{40}Ar/^{36}Ar$ ratios in all four analysed samples (ILR 84-4 #1: $10{,}800\pm2050$;

Table 3
Xe compositions of the same extractions as in Table 1

Extraction[a]	^{132}Xe [10^{-13}][b]	^{129}Xe/^{132}Xe	^{130}Xe/^{132}Xe	^{131}Xe/^{132}Xe	^{134}Xe/^{132}Xe	^{136}Xe/^{132}Xe
ILR 84-4 harzburgite, 6.911 g						
200×	4.08 (4)	0.995 (10)	0.152 (2)	0.790 (8)	0.388 (5)	0.336 (5)
700×	2.93 (3)	1.015 (12)	0.147 (2)	0.789 (10)	0.393 (6)	0.346 (6)
3000×	2.32 (3)	1.012 (14)	0.148 (3)	0.795 (11)	0.396 (5)	0.341 (5)
ILR 84-6 dunite, 5.0384 g						
150×	1.97 (3)	0.995 (13)	0.151 (3)	0.788 (10)	0.397 (7)	0.343 (6)
1000×	2.72 (4)	0.998 (10)	0.151 (2)	0.795 (8)	0.397 (5)	0.337 (5)
3500×	2.01 (3)	0.993 (12)	0.152 (3)	0.791 (10)	0.384 (4)	0.335 (6)
Chisny 88-1 dunite, 7.0461 g						
200×	2.96 (5)	1.009 (8)	0.149 (2)	0.788 (7)	0.403 (5)	0.340 (3)
700×	2.07 (3)	0.998 (11)	0.151 (2)	0.782 (8)	0.396 (5)	0.339 (4)
3000×	2.10 (2)	0.995 (11)	0.151 (3)	0.776 (9)	0.392 (4)	0.343 (5)
AIR		0.983	0.151	0.789	0.388	0.329

Given statistical uncertainties are 1σ and include blank correction and correction for experimentally induced mass fractionation. Again, uncertainty in absolute concentration of calibration gas is considered to be 20%.
[a] Cumulative number of strokes.
[b] In cm^3 STP/g.

ILR 84-4 #2: 9980 ± 1620; ILR 84-6: 8400 ± 1820 (a higher value of 11,700 with a relative uncertainty of ca. 41% is not considered); Chisny 88-1: 11,700 ± 2140). In addition, ILR 84-4 and Chisny 88-1 also have been stepwise crushed in a static crusher. The maximum ratios are 9600 ± 1310 (ILR 84-4) and 9430 ± 730 (Chisny 88-1). Though we cannot ultimately exclude some remaining contributions of atmospheric argon, the very coherent data demonstrate that this contribution must be minor. Previous studies report maximum ^{40}Ar/^{36}Ar ratios of 7973 ± 345 [16] in the same sample ILR 84-4 analysed for this study and 8500 ± 2000 [40], in agreement with our results. However, Hanyu et al. [15] report ^{40}Ar/^{36}Ar ratios of 4408 ± 187 and 4634 ± 427, respectively, accompanied by high ^{20}Ne/^{22}Ne ratios of 12.68 ± 0.12 and 12.64 ± 0.19, in the second and third crushing step of one sample. This result would be in conflict with our data, since it suggests a significant lower ^{40}Ar/^{36}Ar ratio at a mantle ^{20}Ne/^{22}Ne ratio of 12.5. In opposite, their first crushing step is consistent with our mixing trend in Fig. 6 (^{20}Ne/^{22}Ne = 11.22 ± 0.07; ^{40}Ar/^{36}Ar = 2928 ± 73). We therefore could imagine that an argon-rich atmospheric contaminant [28] could have disturbed and lowered the corresponding ^{40}Ar/^{36}Ar ratio.

Our extrapolated ^{40}Ar/^{36}Ar ratio of the mantle component in sample ILR 84-4 is 11,053 ± 220, if ^{20}Ne/^{22}Ne = 12.5 is used. This result is apparently in good agreement with the stepwise heating and stepwise static crushing data described above. In contrast, a ^{20}Ne/^{22}Ne = 13.8 (assumed solar gas composition) would result in an unrealistic high extrapolated ^{40}Ar/^{36}Ar ratio of ~75,000 and r = 0.08. The low r value can be graphically illustrated from extrapolation to ^{20}Ne/^{22}Ne = 13.8 in a ^{36}Ar/^{22}Ne vs. ^{20}Ne/^{22}Ne plot (Fig. 6): The negative slope of the mixing line leads to a decreasing mantle ^{36}Ar/^{22}Ne ratio, whereas the atmospheric ^{36}Ar/^{22}Ne remains the same.

The two mantle endmember ^{20}Ne/^{22}Ne ratios of 12.5 and 13.8 assume two fundamentally different scenarios of the origin of solar noble gases in the Earth, either neon implantation of solar wind ions into Earth's precursor planetesimals [12] or neon capture by a massive proto Earth from the solar nebula (e.g., [41]). Alternatively, some authors suggested hybrid models as a consequence of a two-stage accretion process [42–44]: First, gases from the solar nebula (^{20}Ne/^{22}Ne = 13.8) predominantly trapped in an early phase could be stored now deeply in the Earth supplying the plume endmember. Later accreting asteroidal or cometary material contributed solar wind implanted He and Ne, and planetary Ar components, now thought to be typical for the upper (MORB) mantle. In our mixing model, the Réunion mantle source contains ca. 80% plume neon and 20% MORB neon. Thus, if a solar ^{20}Ne/^{22}Ne ratio of 13.8 ± 0.1 [30] is the correct primordial composition of the plume endmember, a value of ~13.5 is expected for Réunion that corresponds to an extrapolated ^{40}Ar/^{36}Ar ~37,500 (extension of hyperbola in Fig. 6). Such a high value is neither supported by our data nor by previous studies [15,16,18,40].

Thus, our observations strongly favour a Réunion mantle source $^{20}Ne/^{22}Ne$ ratio of about 12.5. This is equivalent to the conclusion that the $^{20}Ne/^{22}Ne$ composition is uniform in the Earth's mantle.

4.2. Understanding global argon–neon and helium–neon systematics

In the following subsection, we consequently use a mantle $^{20}Ne/^{22}Ne$ ratio of 12.5 for air correction of $^{21}Ne/^{22}Ne$- and $^{40}Ar/^{36}Ar$ mantle endmember values.

In the Introduction, we already pointed out that many features of the He–Ne systematics in the oceanic mantle shown in Fig. 1 can be explained by local mixing processes between local plume-type and MORB-type noble gases. While some studies suggest a pure solar composition of the plume component [13], we propose that the plume component is slightly but significantly evolved in radiogenic isotopes [45]. This plume component is not uniform on a global scale but may vary: From Fig. 1, we may deduce a Loihi-type plume endmember (termed P-L in Fig. 1) that is more radiogenic with regard to an Iceland-type plume endmember (P-I in Fig. 1), e.g., displaying $^{4}He/^{3}He$ ratios of 18,000 for P-L and 14,000 for P-I. Both $^{4}He/^{3}He$ endmember compositions would be in accordance with the lowest measured ratios obtained for samples representing the Loihi and Icelandic hotspots [11,19]. The position of the endmembers on the straight line in Fig. 1 requires a different contribution of primordial He and Ne isotopes with a constant $^{3}He/^{22}Ne$ ratio of ca. 7.7, calculated with a $^{4}He^{*}/^{21}Ne^{*}$ production ratio of 2.2×10^{7} [46].

Contrarily, the position on the hyperbola in Fig. 1 is suggested to be due to a recent mixing process. The curvature implies about 10–20 times higher $^{3}He/^{22}Ne$ ratios in the MORB endmember compared to the respective primitive plume endmembers. This is expressed as *r*-L value (for Loihi hyperbola) and *r*-I value (for Icelandic hyperbola) in Fig. 1. Note that the required different $^{3}He/^{22}Ne$ compositions of the Loihi and the Icelandic mantle source in this model are far smaller than deduced by Moreira et al. [13]. Therefore, our model obviates their proposed drastic differences in mixing mechanisms controlled by the geologic setting (i.e., on-ridge and off-ridge). In spite of differences between locally defined mixing hyperbolae, a rather uniform global trend appears to be present, pointing to similar basic processes involved at a global scale. We will return to this point later in Section 4.4.

Similar to $^{21}Ne/^{22}Ne_{mantle}$ and $^{4}He/^{3}He$ systematics in Fig. 1, we can compare the mantle compositions of $^{40}Ar/^{36}Ar$ and $^{21}Ne/^{22}Ne$ of different mantle sources. In Fig. 9, we show estimated $^{40}Ar/^{36}Ar$ reservoir compositions for MORB ($32{,}400 \pm 4200$), Loihi (8000 ± 1000), Iceland (6500 ± 1500) (from compilation in [45]) and the result of this study for the Réunion plume source ($11{,}053 \pm 220$). Note that laser experiments on MORB glass vesicles yielded even higher values of $40{,}000 \pm 6000$ [47]. Thus, the MORB value is still a rough estimate to a certain extent. $^{40}Ar/^{36}Ar$ ratios are plotted against the corresponding mantle $^{21}Ne/^{22}Ne$ ratios (Fig. 9) (MORB: 0.0595 ± 0.0003, Loihi: 0.0362 ± 0.0003, Iceland: 0.0352 ± 0.003, [45]; Réunion: 0.0395 ± 0.0005). Similar to He–Ne systematics (Fig. 1), we observe a characteristic sequence of a correlated, in this case apparently linear, increase in radiogenic/nucleogenic contributions for the respective mantle sources. We might explain these sequence either by different degrees of mixing of a plume and MORB endmember or by a different degree of radiogenic evolution in the respective mantle sources (see below). In any case, the approximate linearity requires a roughly constant $^{36}Ar/^{22}Ne$ ratio in all considered mantle sources until isotopic evolution is complete (i.e., a possible modification of the elemental ratio is restricted to late stage processes). Taking the slope of this mantle trend from Fig. 9 (=1,056,540) and using respective mantle production ratios of $^{4}He^{*}/^{21}Ne^{*} = 2.2 \cdot 10^{7}$ [46] and $^{4}He^{*}/^{40}Ar^{*}=2.5$ (which is in the commonly assumed range of 1–5), we calculate a mantle production ratio of $^{40}Ar^{*}/^{21}Ne^{*} = 8.8 \times 10^{6}$, resulting in a $^{36}Ar/^{22}Ne$ ratio of ~8.3. This agrees well with the

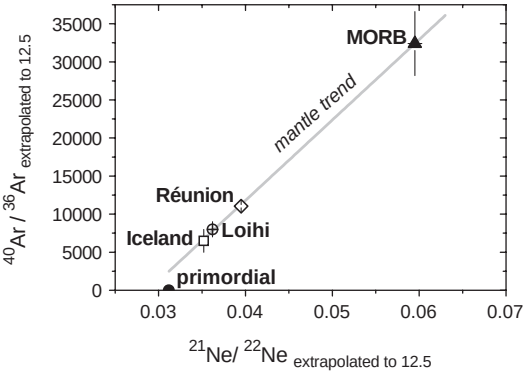

Fig. 9. Combined mantle $^{40}Ar/^{36}Ar$–$^{21}Ne/^{22}Ne$ systematic (extrapolated to $^{20}Ne/^{22}Ne = 12.5$ (Ne–B)). Data for MORB, Loihi and Iceland from Trieloff and Kunz [45] and references therein, Réunion data from this study. Grey line represents a mixing trend between primitive plumes and MORB, or primordial and pure radiogenic, respectively (see text and Fig. 10B), including Réunion. The linearity for all locations shown implies an unfractionated $^{36}Ar/^{22}Ne$ ratio in the corresponding endmember components. Primordial values are $^{40}Ar/^{36}Ar \sim 0$ and $^{21}Ne/^{22}Ne = 0.0312$ (Ne–B [45]).

estimated $^{36}Ar/^{22}Ne$ ratio in this study (~7.6, Fig. 7) and previous determinations of the mantle $^{36}Ar/^{22}Ne$ ratio of about 9.2 ± 3.0 [18,45] (both values at $^{20}Ne/^{22}Ne = 12.5$), independent of sample provenance.

From Fig. 1, we assumed that the Réunion mantle source is affected by a mixing process between a MORB-type and Loihi-type mantle source component, because Réunion and Loihi seem to share a similar mixing hyperbola. Hence, both plume endmembers (Réunion and Loihi) should have experienced a similar isotopic evolution (a_1 in Fig. 10A), before onset of fractionation and mixing, the latter shown schematically as trend a_2 in Fig. 10A that yields the uniform Réunion source composition. However, we may alternatively envisage a slightly different scenario shown in Fig. 10A: initial mixing and/or evolution causes a slightly more radiogenic Réunion endmember (graph b_1), and today Réunion composition is achieved by mixing with MORB following a stronger curved hyperbola (implying stronger He/Ne fractionation) (graph b_2). Note that in both scenarios, the uniform He composition of the Réunion mantle source is achieved by a profound mixing process.

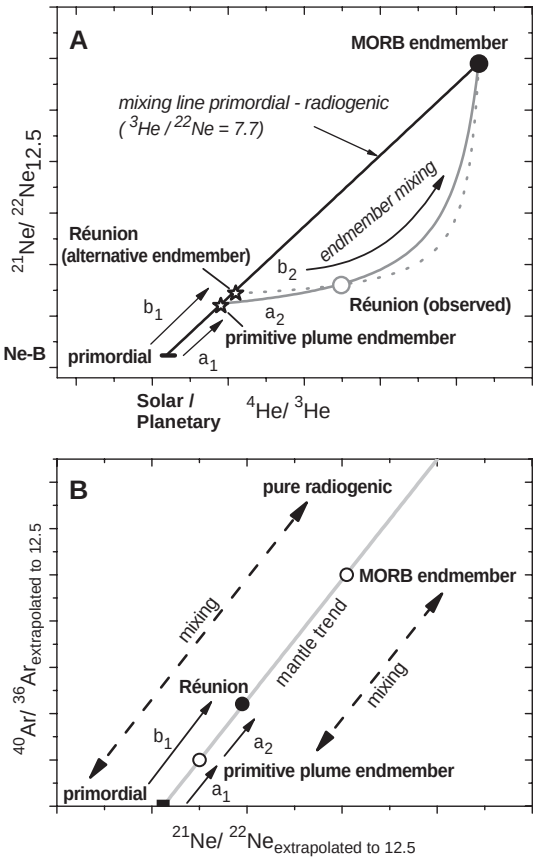

Fig. 10. Schematic overview of (A) He–Ne and (B) Ar–Ne systematics in the mantle. Dashed arrows indicate mixing between a pure radiogenic and a primordial component, and mixing between MORB and a primitive plume endmember, respectively. Letters a_1, a_2, b_1, and b_2 refer to the same processes in both diagrams. Details are given in the text.

The same two scenarios are shown schematically in Fig. 10B for the Ar–Ne system. In scenario $a_{1,2}$ the sampled Réunion mantle source represents a mixture (arrow a_2 in Fig. 10B) between a MORB-type and a plume (Loihi)-type endmember. The latter experienced an isotopic evolution according to graph a_1 in Fig. 10B. The linearity of the obtained mixing trend then immediately point to a negligible degree of fractionation between Ar and Ne in one or both of the respective endmember components. In scenario (b) the more radiogenic character of the Réunion plume source is caused by a stronger admixing of radiogenic ^{40}Ar and nucleogenic ^{21}Ne relative to a Loihi-type plume component (b_1 in Fig. 10B). As mentioned above, in this scenario hardly any MORB-type Ne is present and thus Ar is also very minor affected by contributions of MORB-type Ar. Ar and Ne isotopes then would reflect the pure local Réunion plume endmember that differs from Loihi or Iceland and, hence, will not provide any information about elemental fractionation between Ar and Ne (i.e., no process similar to b_2 in Fig. 10A for He–Ne can be traced). For both scenarios, we want to add that in view of the relative large analytical uncertainties, a linear relationship between mantle $^{40}Ar/^{36}Ar$- and $^{21}Ne/^{22}Ne$ ratios is yet not completely assured, although strongly curved trends can largely be excluded.

4.3. Properties of the two mixing endmember components

From He–Ne–Ar systematics, we can deduce that two major endmember components in the Earth's mantle are present which differ in their relative amount of radiogenic vs. primordial isotopes (Figs. 1, 9, and 10) [35,45,48–50]. Considering the global database, these endmember compositions, here for simplicity termed as MORB and plume component, seem not perfectly homogeneous on a global scale, but rather show limited scatter. In how far this scattering might also be present on a local scale remains open. What is more important is the observation of similar excesses in radiogenic, nucleogenic and fissiogenic isotopes in the MORB component relative to the plume component, no matter if nuclides from long-lived parents (^{40}K, $^{235,\ 238}U$, ^{232}Th) or short-lived parents (^{129}I, ^{244}Pu) are considered [45]. This is best visualized by the observed common

mantle–atmosphere mixing trend in a Xe three-isotope diagram (Fig. 8), that demonstrates a correlated excess of radiogenic ^{129}Xe (from short-lived ^{129}I) and fissiogenic ^{136}Xe (from short-lived ^{244}Pu and long-lived ^{238}U) in all mantle regimes. This is equivalent to similar production ratios of radiogenic, nucleogenic and fissiogenic isotopes in both endmember components. Furthermore, a similar excess of radiogenic isotopes in MORB relative to the plume component also implies a similar elemental ratio of the primordial isotopes in both endmember components. The composition of the endmember components thus can be reduced to be a consequence of mixing between a pure primordial and a pure radiogenic component, but to a different degree in the MORB and plume component, respectively. These reasonings and possible sources of the primordial isotopes (e.g., the core [45,51] or subducted interplanetary dust particles [52]) and radiogenic isotopes are more extensively discussed in [45].

4.4. Primary fractionation

We qualitatively explained the observed hyperbolic isotopic correlation pattern in He–Ne space (Fig. 1) as a two-component mixture between a plume component relatively enriched in primordial isotopes and a shallower mantle component (here designated as MORB) which shows higher relative contributions in radiogenic/nucleogenic isotopes. To obtain a hyperbolic trend in He–Ne space (and He–Ar space, not shown), at least one mantle source has to be fractionated in He relative to Ne and Ar. Furthermore, this fractionation (termed "primary" here) must have occurred after the isotopic composition in the present endmember component was established by time-integrated accumulation of radiogenic/nucleogenic isotopes, since we observe a similar linear radiogenic evolution trend for both endmember components (see grey line in Fig. 1).

It is important to note that the described primary fractionation seems to be a feature of the source region of the melts and may not be confused with late-stage magmatic fractionation events during magma ascent and degassing [9,53–55]. The latter process causes solubility controlled enrichment in He relative to Ne in the course of magma degassing and magma ascent [56,57], i.e., high ^{3}He/^{22}Ne ratios that encompass a range of two orders of magnitude in MORB and Loihi glass samples. Nevertheless, we could imagine that a prior degassing process leads to an increased He/Ne ratio of the MORB source before admixing with melts from an undegassed plume source. This requires an on average uniform degassing of the MORB source to guarantee a rather uniform He/Ne composition of MORB before mixing with plume-related fluids/melts. Otherwise, the strong variations in elemental ratios during the degassing process would blur any simple mixing relations. At odds with this fractionation scenario are the lower He concentrations associated with lower ^{3}He/^{22}Ne ratios in OIB glasses compared to MORB glasses, opposite to the proposed degassed character of MORB—this is one of the so-called He paradoxes [58]. Thus, we also could think of a He deficit in the plume component that would explain the discrepancy between ^{3}He/^{22}Ne ratios and ^{3}He concentrations. In this model, MORB is the essentially unfractionated component. If we assume that mixing of MORB and plume components occurs at a stage where free fluids still have not formed, we could envisage a fractionation during partial melting of the plume related source rocks as the major cause of He deficiency. If He behaves more compatible during partial melting at mantle conditions than Ne and Ar, fractionation would be highest at lowest degree of partial melting, i.e., significant for OIB melts and negligible for MORB melts. Furthermore, Ne and Ar should exhibit similar partition coefficients, as no significant fractionation is detected. The latter is in agreement with a recent study on partition coefficients of Ne and Ar during partial melting of cpx [59], whereas experimental values for He unfortunately do not exist at present. One caveat with this model is the question: where is all this He now that should still be retained in the mantle? This is a serious problem, since retaining the He in the mantle would progressively change the time-integrated isotopic evolution path during Earth's history. Furthermore, the coupling of low degrees of melting, low constant ^{3}He/^{22}Ne ratios and a higher relative contribution of primordial isotopes in the plume component should progressively change with advanced stages of the melting process: With a higher degree of melting, the He/Ne ratio should increase, and hence, in case of an isotopically homogeneous plume source composition mixing of plume-related melts with MORB melts will not result in a simple hyperbolic trend anymore.

This short overview on possible fractionation processes demonstrates that we are still far from understanding the whole processes involved in creating the observed mantle noble gas systematics.

5. Summary and conclusions

Combined measurement of high-precision ^{20}Ne/^{22}Ne and ^{40}Ar/^{36}Ar ratios enabled us to calculate a ^{40}Ar/^{36}Ar ratio of 11,053 ± 220 (dynamic crushing, sample ILR

84-4) using a $^{20}Ne/^{22}Ne$ value of 12.5 representative for the Réunion mantle source. This is consistent with other maximum $^{40}Ar/^{36}Ar$ ratios (9000–11,000) obtained from the same samples by high-resolution stepwise heating and stepwise static crushing that are similar to the calculated value. In addition, this is in agreement with previously reported Ar values (maximum 8500 ± 2000 [38]). In opposite, extrapolation to higher $^{20}Ne/^{22}Ne$ of 13.8 (solar wind [30]) or 13.5 (assuming the Réunion mantle source to be a hybrid mixture between a solar wind type primitive plume component and implanted solar (meteoritic) type MORB) leads to unrealistic high expected $^{40}Ar/^{36}Ar$ ratios of 75,000 and 37,500, respectively. This favours a uniform $^{20}Ne/^{22}Ne$ of about 12.5 in the Earth's interior.

The isotopic composition of Xe in Réunion samples is indistinguishable from previous studies. Analogous to other oceanic samples (MORB, OIB), the obtained $^{129}Xe/^{130}Xe$ and $^{136}Xe/^{130}Xe$ are correlated following the mantle trend and, like other hotpots (Loihi, Iceland), display lower excess in ^{129}Xe and ^{136}Xe relative to MORB. However, it was not possible to evaluate a mantle endmember composition in a way similar to Ar.

We can interpret He–Ne systematics of oceanic mantle sources as two-component mixing between a MORB-type, more radiogenic endmember and a plume-type endmember relatively more enriched in primordial isotopes. Both endmember isotopic compositions can be derived from an initial primordial composition with a $^{3}He/^{22}Ne$ ~7.7 by admixing of radiogenic nuclides.

We extended this approach to the Ar–Ne system and showed that (air-corrected) $^{21}Ne/^{22}Ne_{mantle}$ and $^{40}Ar/^{36}Ar_{mantle}$ ratios of main type localities (MORB, Réunion, Loihi, and Iceland) follow approximately a linear trend. Similar to the He–Ne system, we interpret this as a radiogenic evolution trend of a primordial mantle composition with a $^{36}Ar/^{22}Ne$~8.3. This agrees well with a previously proposed $^{36}Ar/^{22}Ne$ ratio of 9.2 ± 3.0 [18] on the basis of data from oceanic samples. Due to the still poor database for Ar, we cannot exclude a slight fractionation between Ar and Ne between both endmembers.

Acknowledgements

The authors cordially thank Th. Staudacher for providing the samples and W.H. Schwarz for fruitful discussions. Comments from Manuel Moreira and a particular detailed review from Takeshi Hanyu helped considerably to improve the manuscript. This work greatly benefited by the help of M. Falter, E. Burkert, and H. Richter at the MPIK Heidelberg. Special thanks to T. Kirsten and J. Kiko for their support.

References

[1] P. Sarda, Th. Staudacher, C.J. Allègre, Neon isotopes in submarine basalts, Earth Planet. Sci. Lett. 91 (1988) 73–88.
[2] B. Marty, Neon and xenon isotopes in MORB: implications for the earth–atmosphere evolution, Earth Planet. Sci. Lett. 94 (1989) 45–56.
[3] H. Hiyagon, M. Ozima, B. Marty, S. Zashu, H. Sakai, Noble gases in submarine glasses from mid-ocean ridges and Loihi seamount: constraints on the early history of the Earth, Geochim. Cosmochim. Acta 56 (1992) 1301–1316.
[4] M. Moreira, J. Kunz, C.J. Allègre, Rare gas systematics in Popping Rock: isotopic and elemental compositions in the upper mantle, Science 279 (1998) 1178–1181.
[5] T. Dunai, H. Baur, Helium, neon, and argon systematics of the European subcontinental mantle: implications for its geochemical evolution, Geochim. Cosmochim Acta 59 (1995) 2767–2783.
[6] T. Matsumoto, M. Honda, I. McDougall, S. O'Reilly, Noble gases in anhydrous lherzolites from the Newer Volcanics, southeastern Australia: a MORB-like reservoir in the subcontinental mantle, Geochim. Cosmochim. Acta 62 (1998) 2521–2533.
[7] C. Gautheron, M. Moreira, Helium signature of the subcontinental lithospheric mantle, Earth Planet. Sci. Lett. 199 (2002) 39–47.
[8] J. Hopp, M. Trieloff, R. Altherr, Ne isotopes in mantle rocks from the Red Sea region reveal large scale plume–lithosphere interaction, Earth Planet. Sci. Lett. 219 (2004) 61–76.
[9] A.I. Buikin, M. Trieloff, J. Hopp, T. Althaus, E.V. Korochantseva, W.H. Schwarz, R. Altherr, Noble gas isotopes suggest deep mantle plume source of late Cenozoic mafic alkaline volcanism in Europe, Earth Planet. Sci. Lett. 230 (2004/5) 143–162.
[10] M. Honda, I. McDougall, D.B. Patterson, A. Doulgeris, D.A. Clague, Possible solar noble-gas component in Hawaiian basalts, Nature 349 (1991) 149–151.
[11] P.J. Valbracht, Th. Staudacher, A. Malahoff, C.J. Allègre, Noble gas systematics of deep rift zone glasses from Loihi Seamount, Hawaii, Earth Planet. Sci. Lett. 150 (1997) 399–411.
[12] M. Trieloff, J. Kunz, D.A. Clague, D. Harrison, C.J. Allègre, The nature of pristine noble gases in mantle plumes, Science 288 (2000) 1036–1038.
[13] M. Moreira, K. Breddam, J. Curtice, M.D. Kurz, Solar neon in the Icelandic mantle: new evidence for an undegassed lower mantle, Earth Planet. Sci. Lett. 185 (2001) 15–23.
[14] S. Niedermann, W. Bach, J. Erzinger, Noble gas evidence for a lower mantle component in MORBs from the southern East Pacific Rise: decoupling of helium and neon isotope systematics, Geochim. Cosmochim. Acta 61 (1997) 2697–2715.
[15] T. Hanyu, T.J. Dunai, G.R. Davies, I. Kaneoka, S. Nohda, K. Uto, Noble gas study of the Réunion hotspot: evidence for distinct less-degassed mantle sources, Earth Planet. Sci. Lett. 193 (2001) 83–98.
[16] T. Staudacher, P. Sarda, C.J. Allègre, Noble gas systematics of Réunion Island, Indian Ocean, Chem. Geol. 89 (1990) 1–17.
[17] B. Marty, V. Meynier, E. Nicolini, E. Griesshaber, J.P. Toutain, Geochemistry of gas emanations: a case study of the Réunion Hot Spot, Indian Ocean, Appl. Geochem. 8 (1993) 141–152.

[18] M. Trieloff, J. Kunz, C.J. Allègre, Noble gas systematics of the Réunion mantle plume source and the origin of primordial noble gases in Earth's mantle, Earth Planet. Sci. Lett. 200 (2002) 297–313.
[19] F.M. Stuart, S. Lass-Evans, J.G. Fitton, R.M. Ellam, High $^{3}He/^{4}He$ ratios in picritic basalts from Baffin Island and the role of a mixed reservoir in mantle plumes, Nature 424 (2003) 57–59.
[20] M. Moreira, Th. Staudacher, P. Sarda, J.G. Schilling, C.J. Allègre, A primitive plume neon component in MORB: the Shona ridge-anomaly, South Atlantic (51–52°S), Earth Planet. Sci. Lett. 133 (1995) 367–377.
[21] M. Moreira, C.J. Allègre, Helium–neon systematics and the structure of the mantle, Chem. Geol. 147 (1998) 53–59.
[22] P. Sarda, M. Moreira, Th. Staudacher, Rare gas systematics on the southernmost Mid-Atlantic Ridge: constraints on the lower mantle and the Dupal source, J. Geophys. Res. 105 (2000) 5973–5996.
[23] E.T. Dixon, Interpretation of helium and neon isotopic heterogeneity in Icelandic basalts, Earth Planet. Sci. Lett. 206 (2003) 83–99.
[24] T. Althaus, S. Niedermann, J. Erzinger, Noble gases in olivine phenocrysts from drill core samples of the Hawaii Scientific Drilling Project (HSDP) pilot and main holes (Mauna Loa and Mauna Kea, Hawaii), Geochem. Geophys. Geosyst. 4 (1) (2003) 8701, doi:10.1029/2001GC000275.
[25] M.D. Kurz, D. Fornari, D. Geist, J. Curtice, D. Lott, Helium and neon from the deep earth: submarine Galapagos glasses and global correlations, Geochim. Cosmochim. Acta 68 (Suppl. 11S) (2004) A278.
[26] M.D. Kurz, M. Moreira, J. Curtice, D.E. Lott III, J.J. Mahoney, J.M. Sinton, Correlated helium, neon, and melt production on the super-fast spreading East Pacific Rise near 17°S, Earth Planet. Sci. Lett. 232 (2005) 125–142.
[27] C.J. Ballentine, D.N. Barfod, The origin of air-like noble gases in MORB and OIB, Earth Planet. Sci. Lett. 180 (2000) 39–48.
[28] D. Harrison, P. Burnard, M. Trieloff, G. Turner, Resolving atmospheric contaminants in mantle noble gas analyses, Geochem. Geophys. Geosyst. 4 (3) (2003) 1023, doi:10.1029/2002GC000325.
[29] D.C. Black, On the origins of trapped helium, neon, and argon isotopic variations in meteorites: I. Gas-rich meteorites, lunar soils and breccia, Geochim. Cosmochim. Acta 36 (1972) 347–375.
[30] J.P. Benkert, H. Baur, P. Signer, R. Wieler, He, Ne, and Ar from the solar wind and solar energetic particles in lunar ilmenites and pyroxenes, J. Geophys. Res. 98 (1993) 13147–13162.
[31] T. Trull, S. Nadeau, F. Pineau, M. Polvé, M. Javoy, C–He systematics in hotspot xenoliths: implications for mantle carbon contents and carbon recycling, Earth Planet. Sci. Lett. 118 (1993) 43–64.
[32] G.A. Schaeffer, O.A. Schaeffer, ^{40}Ar–^{39}Ar ages of lunar rocks, Proc. Lun. Planet. Sci. Conf. 8th, 1977, pp. 2253–2300.
[33] E.K. Jessberger, W. Gentner, Mass spectrometric analysis of gas inclusions in Muong Nong glass and Libyan Desert glass, Earth Planet. Sci. Lett. 14 (1972) 221–225.
[34] P. Scarsi, Fractional extraction of helium by crushing of olivine and clinopyroxene phenocrysts: effects on the $^{3}He/^{4}He$ measured ratio, Geochim. Cosmochim. Acta 64 (2000) 3751–3762.
[35] M. Ozima, F.A. Podosek, Noble Gas Geochemistry, 2nd ed., Cambridge University Press, Cambridge, 2002, 286 pp.
[36] M. Trieloff, H.W. Weber, G. Kurat, E.K. Jessberger, J. Janicke, Noble gases, their carrier phases, and argon chronology of upper mantle rocks from Zabargad Island, Red Sea, Geochim. Cosmochim. Acta 61 (1997) 5065–5088.
[37] Th. Staudacher, C.J. Allègre, Terrestrial xenology, Earth Planet. Sci. Lett. 60 (1982) 389–406.
[38] J. Kunz, Th. Staudacher, C.J. Allègre, Plutonium-fission xenon found in Earth's mantle, Science 280 (1998) 877–880.
[39] R.J. Poreda, K.A. Farley, Rare gases in Samoan xenoliths, Earth Planet. Sci. Lett. 113 (1992) 129–144.
[40] P.G. Burnard, F. Stuart, G. Turner, C–He–Ar variations within a dunite nodule as a function of fluid inclusion morphology, Earth Planet. Sci. Lett. 128 (1994) 243–258.
[41] D. Porcelli, D. Woolum, P. Cassen, Deep Earth rare gases: initial inventories, capture from the solar nebula, and losses during moon formation, Earth Planet. Sci. Lett. 193 (2001) 237–251.
[42] B. Marty, L. Zimmermann, Volatiles (He, C, N, Ar) in mid-ocean ridge basalts: assessment of shallow level fractionation and characterization of source composition, Geochim. Cosmochim. Acta 63 (1999) 3619–3633.
[43] R. Yokochi, B. Marty, A determination of the neon isotopic composition of the deep mantle, Earth Planet. Sci. Lett. 225 (2004) 77–88.
[44] C.J. Ballentine, B. Marty, B. Sherwood Lollar, M. Cassidy, Neon isotopes constrain convection and volatile origin in the Earth's mantle, Nature 433 (2005) 33–38.
[45] M. Trieloff, J. Kunz, Isotope systematics of noble gases in the Earth's mantle: possible sources of primordial isotopes and implications for mantle structure, Phys. Earth Planet. Inter. 148 (2005) 13–38.
[46] I. Yatsevich, M. Honda, Production of nucleogenic neon in the Earth from natural radioactive decay, J. Geophys. Res. 102 (1997) 10291–10298.
[47] P. Burnard, D. Graham, G. Turner, Vesicle-specific noble gas analyses of "popping rock"; implications for primordial noble gases in Earth, Science 276 (1997) 568–571.
[48] D. Porcelli, G.J. Wasserburg, Mass transfer of helium, neon, argon, and xenon through a steady-state upper mantle, Geochim. Cosmochim. Acta 59 (1995) 4921–4937.
[49] K.A. Farley, E. Neroda, Noble gases in the Earth's mantle, Annu. Rev. Earth Planet. Sci. 26 (1998) 189–218.
[50] D.W. Graham, Noble gas isotope geochemistry of mid-ocean ridge and ocean island basalts: characterization of mantle source reservoirs, in: D. Porcelli, C.J. Ballentine, R. Wieler (Eds.), Noble Gases in Geochemistry and Cosmochemistry, Mineral. Soc. Am., vol. 47, 2002, pp. 247–318.
[51] D. Porcelli, A.N. Halliday, The core as a possible source of mantle helium, Earth Planet. Sci. Lett. 192 (2001) 45–56.
[52] D.L. Anderson, Helium-3 from the mantle: primordial signal or cosmic dust? Science 261 (1993) 170–176.
[53] M. Honda, D.B. Patterson, Systematic elemental fractionation of mantle derived helium, neon, and argon in mid-oceanic ridge glasses, Geochim. Cosmochim. Acta 63 (1999) 2863–2874.
[54] M. Moreira, P. Sarda, Noble gas constraints on degassing processes, Earth Planet. Sci. Lett. 176 (2000) 375–386.
[55] P. Sarda, M. Moreira, Vesiculation and vesicle loss in mid-ocean ridge basalt glasses: He, Ne, Ar elemental fractionation and pressure influence, Geochim. Cosmochim. Acta 66 (2002) 1449–1458.
[56] A. Jambon, H. Weber, O. Braun, Solubility of He, Ne, Ar, Kr, and Xe in a basalt melt in the range 1250–1600 °C, geochemical implications, Geochim. Cosmochim. Acta 50 (1986) 401–408.
[57] G. Lux, The behaviour of noble gases in silicate liquids: solution, diffusion, bubbles and surface effects, with applica-

tions to natural samples, Geochim. Cosmochim. Acta 51 (1987) 1549–1560.
[58] D.L. Anderson, The helium paradoxes, Proc. Natl. Acad. Sci. 95 (1998) 4822–4827.
[59] R.A. Brooker, Z. Du, J.D. Blundy, S.P. Kelley, N.L. Allan, B.J. Wood, E.M. Chamorro, J.-A. Wartho, J.A. Purton, The 'zero charge' partitioning behaviour of noble gases during mantle melting, Nature 423 (2003) 738–741.
[60] M. Moreira, P.J. Valbracht, Th. Staudacher, C.J. Allègre, Rare gas systematics in Red Sea ridge basalts, Geophys. Res. Lett. 23 (1996) 2453–2456.
[61] S. Niedermann, W. Bach, Anomalously nucleogenic neon in North Chile Ridge basalt glasses suggesting a previously degassed mantle source, Earth Planet. Sci. Lett. 160 (1998) 447–462.
[62] M. Moreira, C.J. Allègre, Rare gas systematics on Mid Atlantic Ridge (37–40°N), Earth Planet. Sci. Lett. 198 (2002) 401–416.
[63] P.J. Valbracht, M. Honda, T. Matsumoto, N. Mattielli, I. McDougall, R. Ragettli, D. Weis, Helium, neon and argon isotope systematics in Kerguelen ultramafic xenoliths: implications for mantle source signatures, Earth Planet. Sci. Lett. 138 (1996) 29–38.
[64] C.H. Langmuir, R.D. Vocke Jr., G.N. Hanson, S.R. Hart, A general mixing equation with applications to Icelandic basalts, Earth Planet. Sci. Lett. 37 (1978) 380–392.
[65] W.B. Clarke, M.A. Beg, H. Craig, Excess ^{3}He in the sea: evidence for terrestrial primordial helium, Earth Planet. Sci. Lett. 6 (1969) 213–220.